UV laser-ablated surface textures as potential regulator of cellular response

Prafulla Chandra, Karen Lai,[a] Hak-Joon Sung,[b] N. Sanjeeva Murthy, and Joachim Kohn[c]
New Jersey Center for Biomaterials, Rutgers University, 145 Bevier Road, Piscataway, New Jersey 08854

(Received 30 March 2010; accepted 5 May 2010; published 2 June 2010)

Textured surfaces obtained by UV laser ablation of poly(ethylene terephthalate) films were used to study the effect of shape and spacing of surface features on cellular response. Two distinct patterns, cones and ripples with spacing from 2 to 25 μm, were produced. Surface features with different shapes and spacings were produced by varying pulse repetition rate, laser fluence, and exposure time. The effects of the surface texture parameters, i.e., shape and spacing, on cell attachment, proliferation, and morphology of neonatal human dermal fibroblasts and mouse fibroblasts were studied. Cell attachment was the highest in the regions with cones at ~4 μm spacing. As feature spacing increased, cell spreading decreased, and the fibroblasts became more circular, indicating a stress-mediated cell shrinkage. This study shows that UV laser ablation is a useful alternative to lithographic techniques to produce surface patterns for controlling cell attachment and growth on biomaterial surfaces. © *2010 American Vacuum Society.* [DOI: 10.1116/1.3438080]

I. INTRODUCTION

Effective repair or replacement of damaged tissues requires cells to be able to assemble and organize into a functional structure. Scaffolds that are used to facilitate this process must be designed so that they provide cells with the appropriate cues to promote the desired morphogenesis. Both chemical and physical cues determine the cell behavior near scaffold surfaces. The influence of chemical cues has been investigated the most, and arises from both surface chemistry[1] and molecules dissolved in the medium around the cells, including growth factors and other cytokines. The roles of the physical cues that arise from substrate stiffness[2] and topography[3] were recognized more recently.[3,4] The present study seeks to elucidate the effects of surface feature shape and spacing on cellular response. Understanding the mechanisms that govern cellular response to surface textures will aid in controlling surface properties of biomaterial implants for desired applications.

One of the earliest efforts to control cell adhesion onto biomaterial substrates by modifying topographic features was achieved by texturing Teflon® surfaces by ion etching.[5,6] It was suggested that cells recognized the surface roughness, and the changes in cellular response were attributed to the parameters that characterized the surface roughness.[6] Results showed that cell apoptosis progressively declined when the size of the micropatterned, fibronectin-coated, adhesive islands increased from 75 to 3000 μm^2, and cell spreading was promoted on small (5 μm diameter) islands if they existed as closely spaced clusters.[4] These and other studies show that the substrate topography at micron length scales affects cellular responses. Lithography-based techniques have been by far the most used to produce micro- or nanoscale surface patterns to investigate the effects of size, shape, and spacing of the surface features on cellular responses.[7–11]

Laser has been widely used as a micromachining tool, and the surfaces obtained by this technique have been used to study cell-substrate interactions.[12–15] In contrast to micromachining, we use laser to ablate and modify surfaces as large as 5 cm^2 in a single step without using mask or scanning beams. An intense laser serves as a heat source to rapidly heat a surface and create a few micron thick molten polymer film that produces a texture in the 1–25 μm length scale upon cooling.[16–19] To demonstrate that these features can alter the cellular response, we used poly(ethylene terephthalate) (PET), which has been used in a wide range of biomedical applications such as implantable sutures,[20] surgical mesh,[21,22] vascular grafts,[23] sewing cuffs for heart valves,[24] and components for percutaneous access devices.[6] The results from the measurement of cell attachment, proliferation, and morphology of two fibroblast cell types are presented in this study.

II. MATERIALS AND METHODS

A. Laser ablation

PET films (KRS Plastics, Inc., Tabor City, NC) were used as substrates and ablation was carried out under ambient conditions. Two types of lasers were used. One was a KrF excimer UV laser (Lambda Physik Compex 201), which was operated at 248 nm wavelength with a maximum fluence of 600 mJ/cm^2/pulse, 10 Hz repetition rate (number of pulses per second), and 20 ns pulse width. The beam was 2 $\times 0.5$ cm^2, and samples were placed 2 cm from the exit port. Ablation was carried out at 20–500 mJ/cm^2 fluence, 1–10 Hz repetition rates, and 10–40 pulses. The second laser

[a]Present address: Duke University School of Medicine, Durham, Durham, NC 27701.
[b]Present address: Department of Biomedical Engineering, Vanderbilt University, 5824 Stevenson Center, Nashville, TN 37235.
[c]Author to whom correspondence should be addressed; electronic mail: kohn@biology.rutgers.edu

TABLE I. Parameters of the laser used in preparing the various films used for studying cell response.

Sample	Fluence (mJ/cm^2)	Repetition rate (Hz)	Exposure time (s)
Series R22		Excimer laser	
S1	150	5	2
S2	150	5	4
S3	100	10	2
S4	100	10	4
Series R1		Nd:YAG laser	
	Energy per pulse (mJ); repetition rate fixed at 10 Hz		
S8	19		3
S9	18		4
S11	23		6
S12	23		8

source was a frequency-quadrupled Nd:YAG (yttrium aluminum garnet) laser at 266 nm wavelength. Samples were mounted at ~0.3 m from the exit port. The average beam energy was 22 mJ. Different surface features were obtained by changing the fluence (F, energy per unit area per pulse), repetition rate (f, determines the heat loss between pulses), and pulses (N, exposure time). Eight spots were ablated on each PET film. The details of exposure of each of the films used in this study are given in Table I.

B. Characterization of the surface pattern spacing and shape

Ablated surfaces were examined by optical and scanning electron microscopy (SEM). The surfaces were sputter-coated with gold-palladium using Balzers SCD 004 equipment, and the SEM images were obtained on an AMRAY 18302 electron microscope with the film at 45° to horizontal. The surface pattern spacing in the SEM images was measured using IMAGEJ software (NIH).[25] A total of 25 spots in each of the three distinct regions, cone, ripples, and the transition zone, were measured.

C. Cell attachment and proliferation

The samples listed in Table I with different surface patterns and feature spacings were used. Ablated PET films (0.75×0.45 cm^2) were sterilized under an UV lamp for 1 h. The surfaces were either used directly or, where indicated, were first coated with 2 $\mu g/ml$ of fibronectin (Sigma-Aldrich, St. Louis, MO) for 2 h. The amount of fibronectin coated on the surface was measured through staining with an Alexa Fluor® 594 conjugate fibronectin (Invitrogen, Carlsbad, CA) and fluorescence imaging.

Primary neonatal human dermal fibroblasts (HDFn) (Cascade Biologics, Portland, OR) of passage 5–8 were propagated in Dulbecco's modified eagle medium (DMEM) (Invitrogen Corp., Carlsbad, CA) supplemented with 10% fetal bovine serum (FBS) and 1% penicillin-streptomycin (Invitrogen Corp., Carlsbad, CA). To measure cell attachment, HDFn cells (2×10^4) were labeled with 5 μM CellTracker Green (5-chloromethylfluorescein diacetate) (Molecular Probes, Invitrogen Corp., Carlsbad, CA) and seeded onto PET films. After aspirating the cell culture medium and the unattached cells at 12 h postseeding, the substrates were washed with phosphate buffered saline (PBS). The attached cells were fixed using 4% paraformaldehyde, and nuclei were stained with 2 $\mu g/ml$ Hoechst 33342 (Molecular Probes, Invitrogen Corp., Carlsbad, CA). Fluorescence images were obtained at 492/517 and 355/465 nm (excitation/emission) for CellTracker Green and Hoechst 33342, respectively, using the Zeiss Axiovert D1 inverted fluorescence microscope (Carl Zeiss Inc., Germany). Hoechst-positive nuclei were counted as a cell number using IMAGEJ.

Cell proliferation was measured at 24 h postseeding using the Roche 5-bromo-2-deoxyuridine (BrdU) kit (Roche Diagnostics Corp., Indianapolis, IN). HDFn cells (1×10^4) were seeded onto ablated PET films and incubated for 12 h. Cells were treated with 10 μM of BrdU and incubated for an additional 12 h and fixed with 4% paraformaldehyde. Cells were treated with the anti-BrdU mouse monoclonal antibodies (clone BMG 6H8 IgG1) and nucleases for DNA denaturation in PBS with glycerin for 3 h, followed by a 3 h treatment with sheep anti-mouse-Ig antibodies conjugated to fluorescein. Nuclei were then counterstained with Hoechst 33342 (Molecular Probes) to measure the total number of cells and imaged at 495/517 and 355/465 nm (excitation/emission) for fluorescein-BrdU and Hoechst 33342, respectively, using a fluorescence microscope (Carl Zeiss). BrdU-positive nuclei (proliferating cell number) and Hoechst-positive nuclei (total cell number) were counted using IMAGEJ (NIH).[26] The cell attachment and proliferation per unit area of the sample were determined by normalizing the cell numbers to the area examined in these images.

D. Cell morphology

In addition to HDFn cells used in the attachment and proliferation studies, mouse fibroblasts (NIH3T3) (ATCC, Manassas, VA) were used to measure cell morphological parameters. NIH 3T3 cells were propagated in DMEM

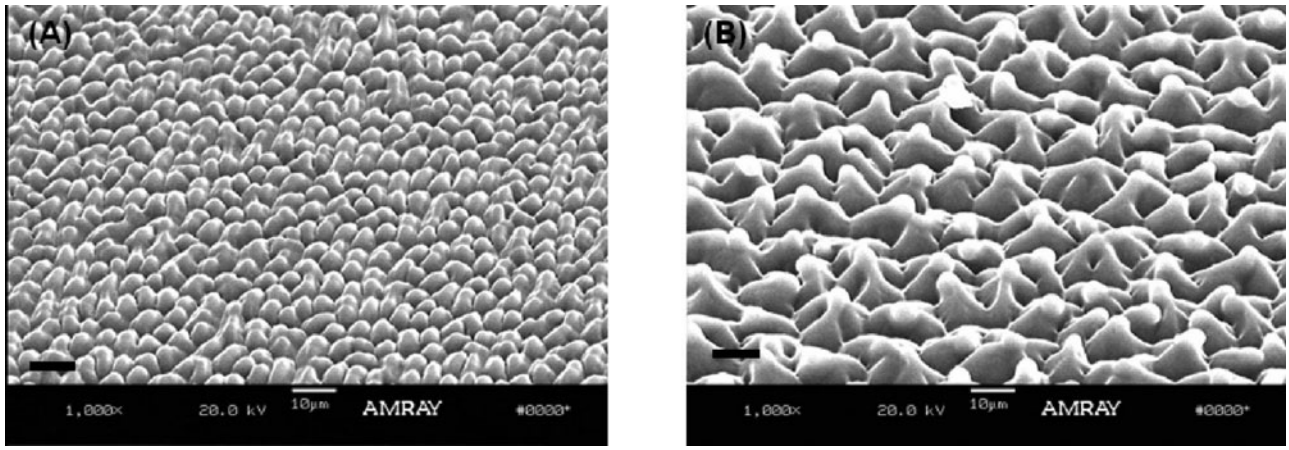

FIG. 1. SEM images of two ablated surfaces of PET. (a) was prepared with a lower laser energy than (b), and both were exposed to Nd:YAG laser for 5 s. Scale bar=10 μm. The images were obtained with the samples tilted at 45°.

supplemented with 10% FBS and 1% penicillin-streptomycin (Invitrogen Corp., Carlsbad, CA). HDFn or NIH 3T3 cells (1×10^3) were seeded onto ablated PET films and incubated for 24 h. Cells were fixed with 4% paraformaldehyde. HDFn cells were stained with Calcein AM (Molecular Probes, Invitrogen Corp., Carlsbad, CA) and nuclei were counterstained with propodium iodide. NIH3T3 cells were stained with fluorescein isothiocyanate (FITC)-phalloidin and nuclei were counterstained with 4′,6-diamidino-2-phenylindole (DAPI). Fluorescence images were obtained under a fluorescence microscope (Carl Zeiss). Ten independent measurements were made and analyzed using IMAGEJ (NIH) to determine the cell area and cell shape.[26]

III. RESULTS AND DISCUSSION

A. Surface pattern spacing and shape

The cone-like surface features obtained by laser ablation of PET films are depicted in Fig. 1. These patterns are generated during the solidification of the thin layer of the polymer that is rapidly melted when the film is illuminated by the high intensity laser during ablation.[19,27] It is estimated that the thickness of the pool of molten material is about 0.1 μm, and the mean temperature gradient is $\sim6\times10^3$ K/μm in strongly UV absorbing polymers such as PET.[28–30] As the top layer of the molten surface cools by being in contact with ambient air, the bottom layers of the melt remain hot, and instabilities occur as a result of local temperature fluctuations. When the local temperature at the free surface becomes higher than the equilibrium temperature, surface tension of the melt decreases locally, and the surrounding cooler regions with a higher surface tension pull the liquid away. As the melt is ejected radially from the heated region to the colder regions, to preserve mass, hot fluid ascends from the lower plane. A system of Marangoni cells whose lateral size ranges from 1 to 10 μm develops wherein fluid ascends near the center of the cells and descends around the periphery. As the polymer cools, these cell arrays become solidified into ripples and cones.

Longer laser exposure time increased the spacing between the surface features. Furthermore, variation in the fluence of the laser beam from the center to the edge gave rise to a gradient in surface patterns [Fig. 2(a)]. Ripples formed near the edge of where the laser fluence was low, whereas cones appeared in the middle where the laser fluence was high. A transition zone between the ripple-filled and cone-filled regions was seen in R1 series films that were ablated with a Nd:YAG laser. The transition zone was not wide enough to be identified as a separate zone in the R22 series that were ablated with the excimer laser.

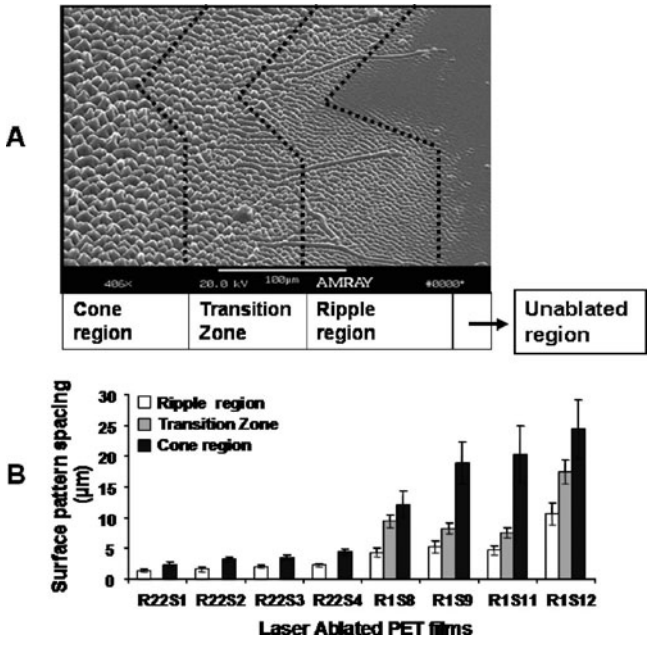

FIG. 2. Surface patterns and the different spacings seen on laser-ablated PET films. (a) A typical SEM image in a R1S12 film, in which four different regions could be identified: the cone, cone ripple in the transition zone, ripple, and nonablated region. Scale bar=100 μm. (b) The surface feature spacing of the various films shown in Table I (n=25). The images were obtained with samples tilted at 45°.

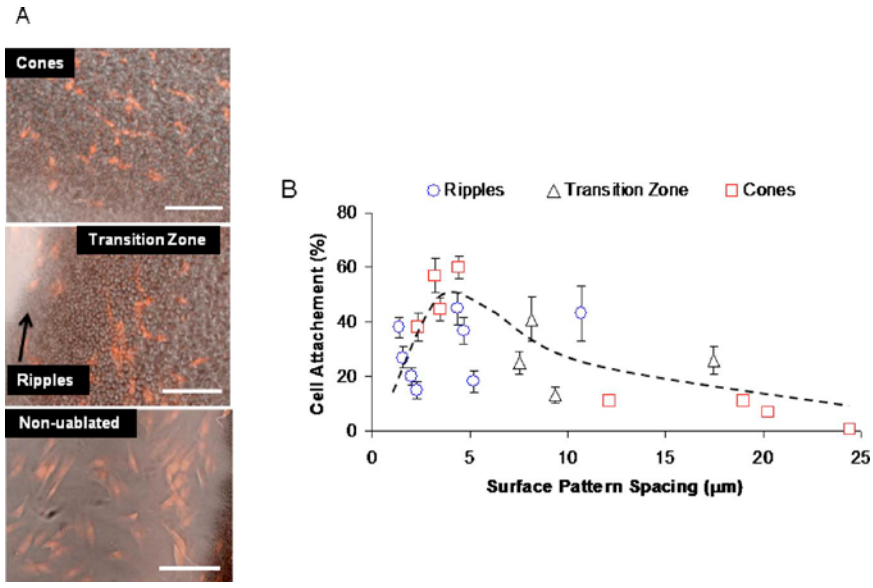

FIG. 3. (Color online) HDFn cell attachment and proliferation on ablated PET films (a) at 24 h postseeding on the R1S9 film. Scale bar=100 μm. (b) Cell attachment at 12 h postseeding in all the films in Table I; the number of cells in each of the regions with different spacings is expressed as a percentage of the total cell number of cells on that film.

At long exposure times, >10 s, the PET films turned brown; holes could be burned through the film and a black char was present at the periphery of the hole. The films that were used for cell experiments were white, and had no evidence of decomposition as confirmed by x-ray photoelectron spectroscopy measurements. Carbonization in these films was found to be minimal as indicated by the carbon to oxygen ratio of 1.11 in the ablated films compared to 1.08 in the nonablated films.

B. Cell attachment and proliferation

Cellular responses to the surfaces such as the ones shown in Fig. 1 were studied. The features are smaller and more closely spaced in Fig. 1(a) compared to the features in Fig. 1(b) (5 vs 15 μm). The attachment of HDFn cells was higher in both of these ablated surfaces relative to nonablated surfaces (84 ± 5 vs 19 ± 10 per mm^2, each value is the number of cells normalized to the area). The results were similar in NIH3T3 cells where the average cell attachment was 80% in the cone regions with 5–10 μm spacing compared to 10%–30% in the nonablated areas. Cells proliferated more (approximately seven times) in the ablated areas compared to the nonablated area in the 5 μm-spacing substrate, but not in the 15 μm-spacing substrate. To explore the effects of feature spacing on cellular responses, samples with different feature spacings were analyzed. The characteristics, the spacing of the cones or ripples, of the eight samples that were used for detailed analysis (Table I) are plotted in Fig. 2(b). In the R1 series, the feature spacing ranged from 4 to 10 μm between the ripples, and from 12 to 24 μm between the cones. The spacing in the R22 series films was smaller: 1–3 μm for the ripples and 2–4 μm for the cones.

The effect of surface topography on cell attachment was studied by analyzing micrographs of cells attached onto the substrates. Figure 3(a) compares the distribution of cells in the nonablated and two types of ablated regions: region with cones and the transition zone. The transition zone between ripples on the left and cones on the right consists of mixture of both ripples and cones, more clearly seen in Fig. 2(a), where the ripples are on the right and the cones are on the left. The number of cells attached to the film (measured at 12 h postseeding) in the cone, ripple, and the transition regions, was calculated as a percentage of the total number of cells in all the three regions (n, number of independent measurements=4). These percentages are plotted in Fig. 3(b) as a function of the feature spacing in all the films. For the cone regions, there is a consistent increase in cell attachment with a decrease in spacing between the cones, i.e., with an increase in surface roughness. However, no such clear trend was observed for the ripples and for the mixed cone-ripple features in the transition zone (Figs. 3 and 4). Thus, the effect of surface roughness appears to be greater when the

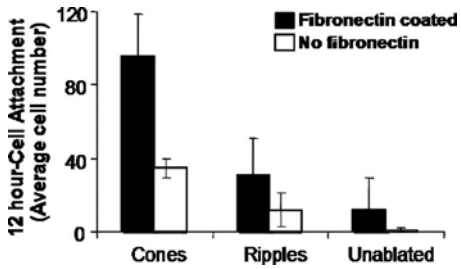

FIG. 4. Comparison of HDFn cell attachment on the ablated R22S4 surface with and without fibronectin coating. Since the transition zone was not wide enough in the R22 films, only cones, ripples, and nonablated regions were analyzed. HDFn cell attachment is presented as an average number of cells attached in each region at 12 h postseeding (n=4).

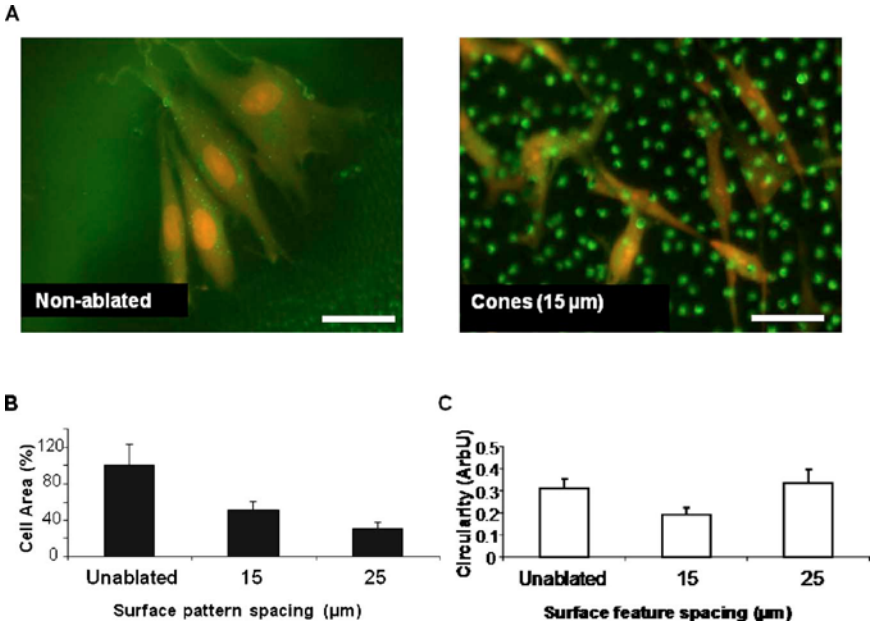

FIG. 5. (Color online) (a) HDFn cell morphology of nonablated and ablated (R1S9) PET films 24 h postseeding. Scale bar is 20 μm. The bright spots are from the tips of the cones. (b) Average cell area in each region is shown as a percentage of the average cell area in the nonablated region (100%). (c) Circularity (a number between 0 and 1, corresponding to a straight line and a circle, respectively) of the cells in the three regions (n=10). R1 series of films were used for plots in (b) and (c).

feature shape was a cone rather than a ripple, indicating cells sensed the shape as well as the feature spacing.

In general, we observed cell attachment to be the highest at 3–5 μm feature spacing, and to be inversely correlated with pattern spacing at spacing >5 μm [Fig. 3(b)]. The cell attachment was lower, even compared to nonablated areas, in regions where the surface features were more than 20 μm apart. When the feature spacing is more than 20 μm apart, which is the average diameter of HDFn cells, it is possible that the cells have no suitable attachment sites, as evidenced by the observed cell shrinkage. The large spacing could have inhibited cell proliferation and caused necrosis (see Sec. III C). This result suggests that as the cells come into contact with a surface, they sense and respond to surface patterns, both the spacing and surface features. Surface topography may provide unique attachment sites in the form of several ripples or cones onto which a single cell attaches. The forced arrangement of these cell adhesion sites can influence the intracellular signaling through focal adhesion molecules such as integrin and focal adhesion kinase, and cytoskeletal molecules such as actin and tubulin. In this way, cell adhesion, cell morphology and behavior are all coupled.

Films coated with fibronectin were examined to evaluate the strength of the influence of surface topography on cellular response, and to mask any chemical differences between the ablated and nonablated surfaces. The comparisons were performed using the R22S4 film (n=4) in which the average spacing in the ripple and cone regions was 3–5 μm, where the highest HDFn cell attachment values were observed [Fig. 3(b)]. The amounts of fibronectin on both the ablated and nonablated surfaces were found to be equal. When the PET surfaces were coated with fibronectin, the attachment of HDFn cells was enhanced on all surfaces, but the trend of increased attachment to textured surfaces remained (Fig. 4). A large increase in the 12 h cell attachment was observed on the nonablated PET films; however, the degree of cell attachment to the ripple and cone textured regions of the film was greater. In the extracellular matrix, fibronectin serves as a cell adhesion molecule by anchoring its adhesive motif to a corresponding receptor on the cell membrane.[31] Its capability of mediating cell-material adhesion has been well documented.[32,33] The current study shows that cell attachment can be modulated by changing the surface topography, even when the same level of surface adhesiveness is maintained by coating the surface with a highly adhesive biomolecule.

C. Cellular morphology

HDFn cell morphology was measured at 24 h postseeding. Figure 5(a) shows that cells in the R1 series of films spread more in the nonablated and transition regions, thus indicating a healthy phenotype,[34] than in the region with cones with ~15 μm spacing. The cell morphology was quantified for the regions with cones for which data over a large range of spacings were available. The cell area in the ablated regions as a percentage of the average cell area in the nonablated region is shown in Fig. 5(b). A decrease in the average cell area from 50% at 15 μm cone spacing to 30% at 25 μm spacing indicates that cell spreading decreases with an increase in surface pattern spacing. The shrinkage of the cells in the cone regions with large spacing was also characterized by fewer peripheral (cytoplasmic) protrusions than the cells in the nonablated regions (and the ripple regions

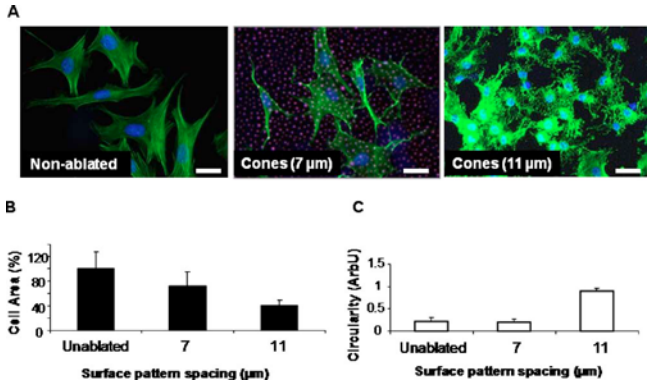

FIG. 6. (Color online) NIH3T3 cell morphology on ablated PET films. (a) At 24 h postseeding. Scale bar=20 μm. The bright spots in the middle picture (7 μm cone spacing) are from the tips of the cones; these were not imaged in the micrographs with 11 μm cone spacing. (b) Average cell area in each region is shown as a percentage of the average cell area in the nonablated region (100%). (c) Circularity, as defined in Fig. 4, of the cells in the three regions (n=10). R1 series of films were used for plots in (b) and (c).

with short spacing; data not shown), indicating a stress-mediated response.[34] A nonablated surface presents unrestricted attachment sites to cells and thus promotes cell spreading albeit in a random way. In contrast, the features (ripples or cones) of an ablated surface serve as attachment sites for a cell and perhaps act as obstacles limiting cell spreading when they are far apart, resulting in fewer contact (attachment) points for the cells. Further studies are needed to clarify this finding.

The shape of the HDFn cells was quantified by measuring their circularity, a number between 0 and 1; 0 corresponding to a straight line and 1 to a circle. A healthy morphology of fibroblasts is indicated by an increase in the peripheral protrusion with dynamic cell extensions comprising tight bundles of long cytoskeleton filaments covered with cell membrane, such as filopodia and lamellapodia.[35] Healthy cells spread more and show less circularity than unhealthy cells in stressful conditions.[36] The results for the nonablated, ripple, and cone regions are shown in Fig. 5(c). Interestingly, the lowest circularity was seen in the cells on the region with 15 μm spacing. As the spacing increased to 25 μm, the circularity increased up to the same level as that in the nonablated regions but the cell area decreased, indicating a stress-mediated cellular response to the cone region while dying, as can be seen visually in Fig. 5(a).

NIH3T3 mouse embryonic fibroblasts showed a similar trend in their morphological changes (Fig. 6). In addition to cell shrinkage, the organization of the actin cytoskeleton of in these cells was affected while growing in the cone regions [Fig. 6(a)]. Bright fluorescence intensity from the actin staining observed in the cells in the cone regions indicates actin polymerization derived from cell stress and death.[37] Figure 6(b) shows that cell area decreased to ~40% with the increase in pattern spacing to 11 μm, 100% being the average cell area on nonablated regions. The change in circularity in NIH 3T3 cells [Fig. 6(c)] was somewhat different from those observed in HDFn cells. The circularities of the NIH 3T3 cells in the nonablated region and in cone regions with 7 μm spacing were about the same. However, the circularity increased dramatically as the spacing increased to 11 μm, indicating a stress-mediated cell response or death,[26] as can be seen visually in Fig. 6(a).

IV. CONCLUSIONS

Laser ablation, unlike lithographic techniques, can be used to rapidly and inexpensively texture complex surfaces and thus are useful in modulating cellular response to biomaterial surfaces. Topographical features at 1–25 μm length scales were produced on PET surfaces by controlling fluence, pulse repetition rate of either an excimer or a Nd:YAG laser, and exposure time. Cell attachment (HDFn) was found to be highest with cones spaced 3–5 μm apart, whereas cones or ripples spaced 20–25 μm apart inhibited cell attachment and proliferation. It is concluded that the shape and length scale of the surface features, both of which can be controlled using the techniques described here, can be used to study the mechanisms that direct cellular responses to surfaces and also to control cellular interactions with implantable medical devices.

ACKNOWLEDGMENTS

The authors would like to thank R. L. Headrick for the use of the excimer laser, F. Zimmermann for the use of the Nd:YAG laser, A. Howe and D. Washington for preliminary cell culture work, and C. Florek for reviewing the manuscript. This work was supported by NIH Grant No. P41 EB001046 (RESBIO: integrated resources for polymeric materials) to the New Jersey Center for Biomaterials, and by Cottrell College Science Award No. CC6394 from Research Corporation.

[1]B. G. Keselowsky, D. M. Collard, and A. J. Garcia, Biomaterials **25**, 5947 (2004).
[2]F. X. Jiang, B. Yurke, B. L. Firestein, and N. A. Langrana, Ann. Biomed. Eng. **36**, 1565 (2008).
[3]J. Tan and W. M. Saltzman, Biomaterials **25**, 3593 (2004).
[4]C. S. Chen, M. Mrksich, S. Huang, G. M. Whitesides, and D. E. Ingber, Science **276**, 1425 (1997).
[5]Z. W. Kowalski, Vacuum **63**, 603 (2001).
[6]A. F. von Recum, J. Biomed. Mater. Res. **18**, 323 (1984).
[7]R. Singhvi, A. Kumar, G. P. Lopez, G. N. Stephanopoulos, D. I. C. Wang, G. M. Whitesides, and D. E. Ingber, Science **264**, 696 (1994).
[8]S. N. Bhatia, M. L. Yarmush, and M. Toner, J. Biomed. Mater. Res. **34**, 189 (1997).
[9]Y. Ito, Biomaterials **20**, 2333 (1999).
[10]C. D. McFarland, C. H. Thomas, C. DeFilippis, J. G. Steele, and K. E. Healy, J. Biomed. Mater. Res. **49**, 200 (2000).
[11]C. D. W. Wilkinson, M. Riehle, M. Wood, J. Gallagher, and A. S. G. Curtis, Mater. Sci. Eng., C **19**, 263 (2002).
[12]P. Li, U. Bakowsky, F. Yu, C. Loehbach, F. Muecklich, and C. M. Lehr, IEEE Trans. Nanobiosci. **2**, 138 (2003).
[13]A. H. Thissen, A. J. P. Hayes, A. P. Kingshott, A. G. Johnson, A. E. C. Harvey, and A. H. J. Griesser, Smart Mater. Struct. **11**, 792 (2002).
[14]S. Iwanaga, Y. Akiyama, A. Kikuchi, M. Yamato, K. Sakai, and T. Okano, Biomaterials **26**, 5395 (2005).
[15]M. Yamato, C. Konno, S. Koike, Y. Isoi, T. Shimizu, A. Kikuchi, K. Makino, and T. Okano, J. Biomed. Mater. Res. **67A**, 1065 (2003).
[16]V. V. Semak and N. B. Dahotre, *Surface Engineering Series: Lasers in Surface Engineering* (ASM International, Materials Park, OH, 1998), Vol. 1, pp. 35–67.

[17]N. Bityurin, B. S. Luk'yanchuk, M. H. Hong, and T. C. Chong, Chem. Rev. **103**, 519 (2003).
[18]T. Lippert and J. T. Dickinson, Chem. Rev. **103**, 453 (2003).
[19]N. S. Murthy, J. J. Martin, R. D. Prabhu, L. Zhou, and R. L. Headrick, J. Appl. Phys. **100**, 023538 (2006).
[20]C. C. Chu and Z. Kizil, Surg. Gynecol. Obstet. **168**, 233 (1989).
[21]U. Klinge, B. Klosterhalfen, J. Conze, W. Limberg, B. Obolenski, A. P. Öttinger, and V. Schumpelick, Eur. J. Surg. **164**, 951 (1998).
[22]B. M. Soares *et al.*, J. Biomed. Mater. Res. **32**, 293 (1996).
[23]G. Riepe *et al.*, Eur. J. Vasc. Endovasc Surg. **13**, 540 (1997).
[24]K. Tweden, J. D. Cameron, A. Razzouk, W. Holmberg, and S. Kelly, J. Heart Valve Dis. **6**, 553 (1997).
[25]M. Abramoff, P. Magalhães, and S. Ram, Biophotonics Int. **11**, 36 (2004).
[26]H. J. Sung, S. G. Eskin, Y. Sakurai, A. Yee, N. Kataoka, and L. V. McIntire, Ann. Biomed. Eng. **33**, 1546 (2005).
[27]D. Isvoranu and M. D. Staicovici, Int. J. Heat Mass Transfer **47**, 3769 (2004).
[28]T. Bahners and E. Schollmeyer, J. Appl. Phys. **66**, 1884 (1989).
[29]C. W. Kan, J. Appl. Polym. Sci. **107**, 1584 (2008).
[30]T. Textor, T. Bahners, and E. Schollmyer, J. Ind. Textiles **32**, 279 (2003).
[31]R. Pankov and K. M. Yamada, J. Cell. Sci. **115**, 3861 (2002).
[32]A. J. Bergman and K. Zygourakis, Biomaterials **20**, 2235 (1999).
[33]A. Mardilovich, J. A. Craig, M. Q. McCammon, A. Garg, and E. Kokkoli, Langmuir **22**, 3259 (2006).
[34]H. J. Sung, P. Chandra, M. D. Treiser, E. Liu, C. P. Iovine, P. V. Moghe, and J. Kohn, J. Cell. Physiol. **218**, 549 (2009).
[35]M. P. Corriveau *et al.*, J. Pathol. **217**, 534 (2009).
[36]M. D. Treiser, E. Liu, R. A. Dubin, H. J. Sung, J. Kohn, and P. V. Moghe, BioTechniques **43**, 361 (2007).
[37]M. R. Bubb, I. Spector, B. B. Beyer, and K. M. Fosen, J. Biol. Chem. **275**, 5163 (2000).